ORIGINAL PAPER

A label-free electrochemical biosensor based on PBA-Au-MXene QD for miR-122 detection in serum samples

Sara Ranjbari[1] · Behnaz Hatamluyi[2] · Seyed Hamid Aghaee-Bakhtiari[3] · Majid Rezayi[4,5] · Reza Arefinia[1]

Abstract

A poly(n-butyl acrylate)-gold-MXene quantum dots (PBA-Au-MXene QD) nanocomposite-based biosensor is presented that is modified by unique antisense single-stranded DNA (ssDNA) and uses the electrochemical detection methods of DPV, CV, and EIS to early detect miR-122 as a breast cancer biomarker in real clinical samples. This fabrication method is based on advanced nanotechnology, at which a poly(n-butyl acrylate) (PBA) as a non-conductive polymer transforms into a conductive composite by incorporating Au-MXene QD. This biosensor had a limit of detection (LOD) of 0.8 zM and a linear range from 0.001 aM to 1000 nM, making it capable of detecting the low concentrations of miR-122 in patient samples. Moreover, it allows approximately 100% sensitivity and 100% specificity for miR-122 without extraction. The synthesis and detection characteristics were evaluated by different complementary tests such as AFM, FTIR, TEM, and FESEM. This new biosensor can have a high potential in clinical applications to detect breast cancer early and hence improve patient outcomes.

Introduction

The capability to identify the extremely low tiers of circulation miRNAs (microRNA) in the blood is critical for creating liquid biopsies that can identify disease progression, like cancer or resistance to therapy before it appears on an image scan. Besides the advantages of rapid and readily reproducible testing, liquid biopsies might be utilized to detect cancer signals earlier, before symptoms occur. This has the potential to significantly impact how we approach and remedy cancer [1, 2]. For example, Saleh et al. [3] showed that miR-122 (miRNA-122) is significant as a diagnostic marker in the screening, diagnosis, and therapy analyses of breast cancer (BC). The magnitude of the circulation miR-122 level is an efficient technique for forecasting metastases in BC patients; it also determines the choice of therapeutic methods employed. High miR-122 levels in the blood have been associated with metastases in BC patients. For the cancer patient, a blood test to measure circulation miR-122 levels would allow researchers to track the effectiveness of the treatment [4].

The current gold standard methods for detecting miR-NAs lean on real-time polymerase chain reaction (RT-qPCR). While it is not consistent with detecting miRNA effectively in the whole circulation, the ability of RT-qPCR is its specificity and selectivity. RNAs must be extracted and purified before RT-qPCR analysis of samples, and cDNA must be synthesized to evaluate miRNA expression. However very dependable, this approach is a time-consuming and complicated labor operation. Specific assessment of clinical specimens would reduce specimen damage while offering a faster and more flexible diagnostic test [5].

Majid Rezayi is the corresponding author who died while conducting the research.

✉ Reza Arefinia
    arefinia@um.ac.ir

1   Chemical Engineering Department, Faculty of Engineering, Ferdowsi University of Mashhad, Mashhad, Iran

2   Antimicrobial Resistance Research Center, Mashhad University of Medical Sciences, Mashhad, Iran

3   Department of Medical Biotechnology and Nanotechnology, Faculty of Medicine, Mashhad University of Medical Sciences, Mashhad, Iran

4   Cancer Research Center, Shahid Beheshti University of Medical Sciences, Tehran, Iran

5   Department of Medical Biotechnology, Faculty of Medicine, Mashhad University of Medical Sciences, Mashhad, Iran

Direct analysis procedures are significant because they can minimize bias in the population of extracted RNA sequences induced by factors such as poor extraction integrity owing to RNA disintegration during separation. As a result, it is necessary to develop point-of-care technologies that can directly detect miRNAs [5].

Since molecular detection methods are limited, developing innovative diagnostic procedures, like biosensors, is necessary to detect early diseases. As a consequence, biochemical approaches could help the early detection based on the biomarker diagnosis and quantification [6]. In this regard, electrochemical biosensors have many advantages such as instrumentation, flexibility, sensitivity, simplicity, transportability, low cost, integration ease, downsizing, and signal stability [7].

Various nanoparticles such as gold, carbon nanotubes, noble metal nanoparticles, graphene, and MXene have been used to improve the wide linear range, and the limit of detection (LOD) of the electrochemical biosensors through their high surface-to-volume ratio, biomedical suitability, and resistance to unfavorable environments [8, 9]. For example, Ebrahimi et al. [10] designed an electrochemical biosensor utilizing gold nanorod and graphene oxide (GO) nanocomposite design to detect miRNA-199a-5p as a BC biomarker. The detection linear range of this biosensor was from 15 fM to 148 pM with an LOD of 4.5 fM. In another study, Liu et al. [11] designed an electrochemical biosensor based on molybdenum disulfide (MoS_2)@Au nanocomposite to detect miRNA-155 with a linear range from 1 fM to 10 nM and a LOD of 0.32 fM. They showed that controlling their morphology and thickness is critical to achieving hypersensitive detection signals.

miR-122 has been used for BC identification in previous studies [12, 13]; however, attaining a wide linear range and a lower LOD is still a challenge to increase detection efficiency. To this goal, this study concentrated on the construction of a new free-label electrochemical biosensor based on Au-MXene QD nanocomposite for miR-122 detection as a biomarker for BC, to direct diagnosis in serum samples without the requirement for extraction. Moreover, using basic nanotechnology methods, PBA as a non-conductive polymer was improved into a conductive nanocomposite with Au-MXene QD for BC detection. The initial phase of the process was the one-step synthesis of Au nanostructures on the MXene surface. The second phase was the electrochemical synthesis of the PBA-Au-MXene QD nanocomposite. Then the ssDNA probe oligonucleotide sequences were linked to gold nanoparticles such that miR-122 could be easily hybridized with the ssDNA probe. To test the biosensor's performance, different electrochemical methods including electrochemical impedance spectroscopy (EIS), cycle voltammetry (CV), and differential pulse voltammetry (DPV) were utilized. Finally, a comparison was made between the selectivity and sensitivity of the suggested miR-122 biosensor in serum samples without pretreatment and an RT-qPCR analysis.

Section of experimental

Instruments and reagents

The supplementary file includes detailed descriptions of the chemicals and apparatus.

MXene QD synthesis

Synthesis of MXene QD is explained in the supplemental file.

Au-MXene QD preparation

The one-step method used to create Au-MXene QD is explained in the supplemental file.

PBA-Au-MXene QD preparation and sensing platform design

In the first stage, the glassy carbon electrode (GCE) was polished with a 0.3 μm alumina slurry, followed by sonication in a mixture of ethanol and water of equal volume. The PBA-Au-MXene QD composite was electrodeposited on the GCE at the potential of -1.15 V for 300 s according to the chronoamperometry approach [14]. To do this, 5 mL of water-based electrolyte including 2 M nBA (monomer), 0.01 M HDDA (inhibitor), 8000 ppm Au-MXene QD (inhibitor), and 0.04 M HEMA (crosslinker) was used, and the pH of the resultant solution was fixed to 6 by adding solid NaOH. The electrolyte was purged with N_2 for 15 min before electrodeposition to make an oxygen-free state. After that, 6 μL of thiolated ssDNA as the probe, with a 500 nM concentration, prepared in 0.05 M PBS (comprising 0.1 M NaCl, pH 7.4), was dropped on the surface of PBA-Au-MXene QD/GCE for 7 h to stabilize the ssDNA probe. To remove the unbonded ssDNA probe, PBA-Au-MXene QD/GCE was rinsed with PBS (0.2 M). Finally, the non-proprietary binding site was blocked with 6 μL of BSA (1% wt) for 30 min and then rinsed with PBS. The FTIR, TEM, FESEM, and EDX analyses were used to investigate the chemical characteristics, chemical bonding, and morphology of the synthesized MXene QD, n-BA monomer, and PBA-Au-MXene QD.

Electrochemical detection and measurement of miR-122

The hybridization process of the ssDNA/PBA-Au-MXene QD/GCE with miR-122 was performed by incubation for 1 h in PBS solution (0.05 M, pH 7.4) containing 0.1 M NaCl and different miR-122 concentrations. To detect miR-122, 5 mM ferricyanide comprising 0.1 M KCl (as an electrolyte) was used as an electrochemical indicator in this study. The drop

in ferrocyanide peak current after hybridization is caused by the electrostatic expulsion process of the DNA/RNA duplex and redox couple in this assay.

The redox DPV signal was conducted at −0.2 to 0.4 V in ferrocyanide solutions with a scan rate of 50 mVs^{-1}, modulation time of 50 ms, and a pulse amplitude of 50 mV. EIS and CV were used to examine the electrochemical properties in 5 mM ferrocyanide comprising 0.1 M KCl. EIS measurements were taken with an amplitude of 10 mV and a frequency range of 0.01 Hz to 100 kHz. Voltammograms of CV were recorded between −600 and +600 mV at a scan rate of 150 mVs^{-1}.

Extraction of miRNA, cDNA synthesis, and RT-qPCR analysis

To perusal and approval of the biosensor method for real specimens, 30 serum specimens (collected from an established bank at Qaim Hospital, Mashhad, Iran, dependent on the research projects approved by the MUMs ethics committee, and affirmed by RT-qPCR and mammography). The supplemental file describes the extraction of miRNA, the synthesis of cDNA, and the RT-qPCR method.

A reliable technique for extracting and amplifying miRNAs from specimens was recently described without the need for complicated extraction methods, time-consuming processes, solvent stage separations, and costly and hazardous chaotropic chemicals [15]. For the analysis of 30 serum specimens, 10 μL of proteinase K (20 g.L^{-1}) and 1 mg of CaCl$_2$ were added to 490 μL of serum, followed by incubation for 10 min at 50 ℃ before analysis [15, 16]. Scheme 1 depicts the preparation of an offered biosensor for the identification of real samples from BC patients. The biosensor was compared to RT-qPCR analysis in extracted and non-extracted samples.

The investigation's subsequent trials focused on the biosensor's capabilities. The biosensor's ability to detect diluted miRNA extracted from clinical samples was evaluated for this reason. The ssDNA/PBA-Au-MXene QD/GCE hybridization procedure was carried out by incubating for 1 h in 0.05 M PBS solution (pH 7.4) containing 0.1 M NaCl at a dilution of 1:10^{12} (1 pM) of without/with extracted miRNA samples.
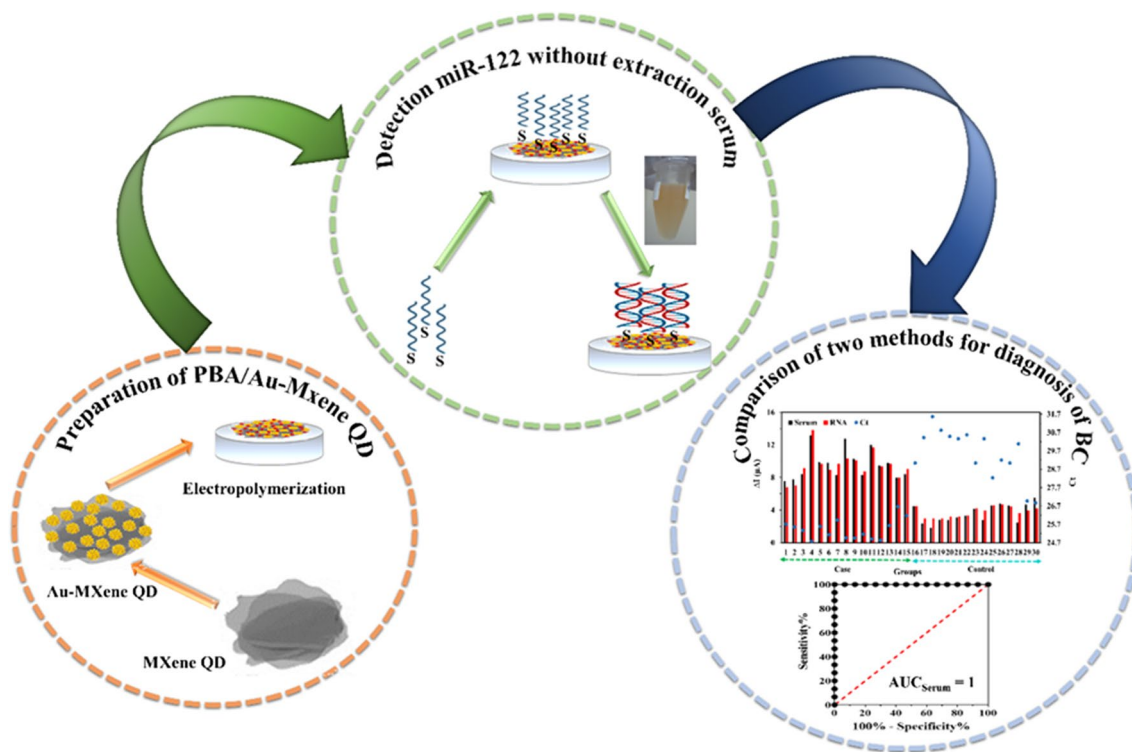

Scheme1 The preparation of a biosensor for the identification of real samples from BC and the comparison between RT-qPCR analysis and biosensor in extracted and non-extracted samples

Results and discussion

The biosensor's chemical and physical characteristics

The FTIR spectra of MXene QD are shown in Fig. 1A (curve a). As seen, tensile vibrational bonds of 3185, 3615, and 3733 cm^{-1} are mostly connected to hydroxyl groups [17, 18], and the vibrational bonds 2294 and 2829 cm^{-1} are associated with the O and H groups, respectively. Aside from the C=O bond at 2252 and 2337 cm^{-1}, the flexural vibrational has a bond at 1575 cm^{-1} owing to the existence of OH (molecular water), which is absorbed by external water owing to the hydrophilic character of MXene QD [17, 18]. Cations of Ti^{+4} can be related to the vibration states of the separate hydroxyl groups [17, 19]. The bond at 919 cm^{-1} shows Ti-C out-plate vibrations (twisting or shaking) [20]. The highest absorption of TiO$_2$ is 474 cm^{-1} [20].
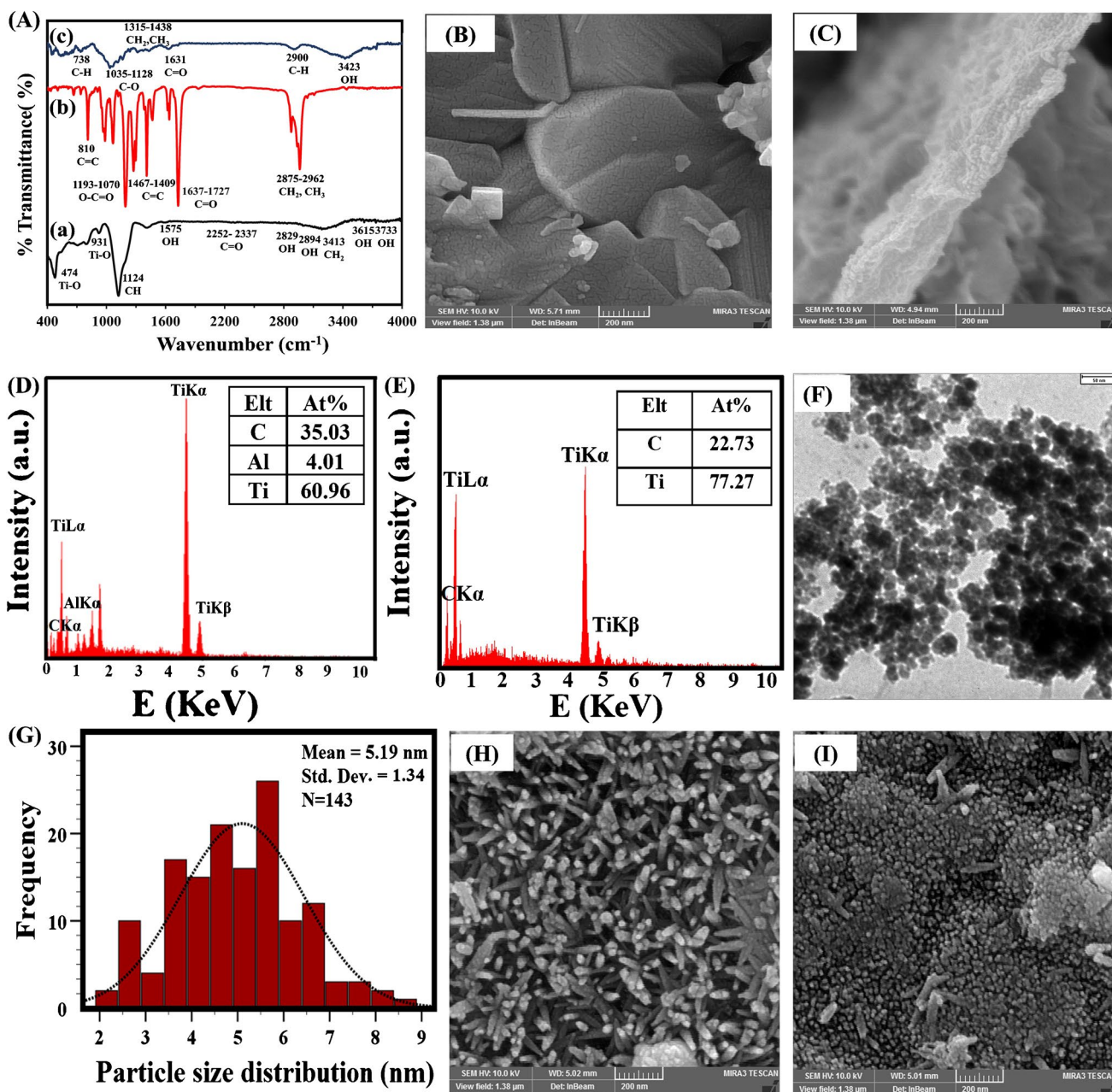
Fig. 1 **A** FTIR spectra of **(a)** MXene QD **(b)** nBA monomer **(c)**PBA-Au-MXene QD, **B** and **C** FESEM image of MAX phase and MXene QD (magnification 200 nm), **D** and **E** EDX of MAX phase and MXene QD, **F** TEM of MXene QD (magnification 50 nm), **G** plot of MXene QD particle size distribution, and **H** and **I** FESEM image of Au-MXene QD with concentration 2 mM and 0.2 mM

Figure 1B and C show a FESEM illustration of Ti_3AlC_2's blocky morphology as the result of effective MAX phase exfoliating. The EDX analysis findings also demonstrate that the Al element has been eliminated and that Ti and C elements are present in the MXene QD nanostructure (Fig. 1D and E). From the TEM imaging in Fig. 1F, nanostructured MXene QD is clear, indicating that the structure is narrow. The produced MXene QD nanostructures are around 5.19 nm in size (Fig. 1G) which shows that MXene is a quantum dot. Figure 1H reveals that morphologies of flowers were formed for Au (2 mM concentration) on MXene QD, but at low concentrations of Au (0.2 mM), no flower morphologies were generated (Fig. 1I)

The FTIR spectra of monomer and PBA-Au-MXene QD nanocomposite are displayed in Fig. 1A with the assignment of their characterized adsorption bonds. On the spectrum of the n-BA monomer (Fig. 1A curve b), we observed the O–H at 3438 cm^{-1} [21] and C-H stretching vibration of CH_2 and CH_3 between 2875 and 2962 cm^{-1}, C=C vinyl carbons vibration between 1409–1467 and 810 cm^{-1}, and vibrations of ester group in 1070–1193 cm^{-1} were beheld [22]. When acrylate suspension is exposed to constant voltage in the attendance of an electrochemical initiator, free radical polymerization occurs rapidly, resulting in polymer networks. Figure 1A curve c illustrates the FTIR spectra of PBA-Au-MXene QD. The bond at 3423 cm^{-1} indicates the presence of the O–H group [21]. C-H stretching vibration at 2900 cm^{-1} and bending vibrations in the C-H plane 1315 and 1438 cm^{-1} are attributed to CH_2 and CH_3, respectively. Stretching vibrations in the C=O group were observed at 1631 cm^{-1}, and the bond at 1035–1128 cm^{-1} confirmed the C-O group's presence [21, 23]. In addition, a reduction in intensity was observed in C–C stretching vibrations at 1625 cm^{-1} and CH out-of-plane bending mode at 738 cm^{-1}. Removing multiple acrylate bonds 1637, 1618, 1409, 985, and 810 cm^{-1} confirmed complete polymerization [21, 24].

The original and modified GCE morphology was studied using FESEM in the second stage. FESEM imaging comparing GCE and PBA-Au-MXene QD (Fig. S1A and B) reveals that an electrosynthesis layer of PBA-Au-MXene QD composite produced on the GCE area was effectively built. The mapping study provided additional confirmation of the PBA-Au-MXene QD biosensing platform, as shown in Fig. S1C, 1D, 1E, and 1F. They equally dispersed the C, Au, O, and Ti elements over the GCE area.

AFM was utilized to investigate changes in the GCE area following modification by PBA-Au-MXene QD, probe, and hybridization. Fig. S2 depicts the tap method of 3D AFM topographical characteristics as well as the 2D phases of the AFM's GCE and modified GCEs. The R_a (average roughness) and R_q (root square roughness) of GCE (Fig. S2A) and PBA-Au-MXene QD/GCE (Fig. S2B) decreased significantly, from 165.27 to 26.28 nm and 206.68 to 35.28 nm, respectively. GCE has uneven depressions and fossa, and most of the depressions and fossa are filled and sensible by a revised PBA-Au-MXene QD [25].

Following the probe's stabilization, the surface morphology has been altered by amounts of R_a 59.21 nm and R_q 74.02 nm (Fig. S2C), and by having to add thiolated ssDNA to the surface, it has become rougher, confirming the achievement of covalent bonds among -S probe groups and Au [26]. After incubating the probe with miR-122 to generate a dsDNA that completely covers the functionalized GCE area, R_a and R_q levels were enhanced to 128.52 nm and 165.17 nm, respectively (Fig. S2D).

Electrochemical analysis

The entire DNA biosensor platform manufacturing process was validated using CV and EIS methods with a reversible redox probe off 5 mM $[Fe(CN)_6]^{3-/4-}$ solution comprising 0.1 M KCl. Using a tantamount Randles circuit, the impedance spectra of all stages were examined. Nyquist is made up of two segments: semicircular and linear. Resistance transfer charges (R_{ct}), the semicircular segment diameter representing the span transitions, control the GCE area in the high-frequency span [27].

When PBA-Au-MXene QD was electrodeposited on GCE ($R_{ct} = 59.23 \pm 0.001$ kΩ) (Fig. 2A and B curve a), there was a considerable increment in redox current (Fig. 2A, curve b) and a decrease in R_{ct} to 0.78 ± 0.006 kΩ (Fig. 2B, curve b), indicating that the electron process of transition had already been enabled because of the active surface area of the electrode and enhanced permeability. The redox current was reduced (Fig. 2A, curve c) and the R_{ct} amount gained to 0.90 ± 0.002 kΩ whenever the oppositely charged phosphate scaffold of the probe was bound on the PBA-Au-MXene QD/GCE area, and the electron transfer was constrained due to electrostatic interaction (Fig. 2B, curve c). The redox current was dramatically decreased after hybridization between the miR-122 and the probe (Fig. 2A, curve d). The R_{ct} value increased to 4.65 ± 0.005 kΩ (Fig. 2B, curve d) as a result of negative charge limiting components and reduced charge species accessibility to the biosensing system area [28]. Both the EIS and CV approaches revealed that the miR-122 sensor platform was successfully manufactured.

A series of CV measurements with varied scan speeds (10 to 150 mV.s^{-1}, a reversible redox probe off 1 mM $[Fe(CN)_6]^{3-/4-}$ solution comprising 0.1 M KCl) was done to evaluate the effective surface area quantity of different electrodes using the Randles–Sevcik Eq. (29) . Both GCE and PBA-Au-MXene QD/GCE electrodes displayed a linear solidarity between the resultant peak currents of anodic and scan rate square roots (Fig. S1G), confirming that the electrochemical reaction is by diffusion rein [29]. Utilizing
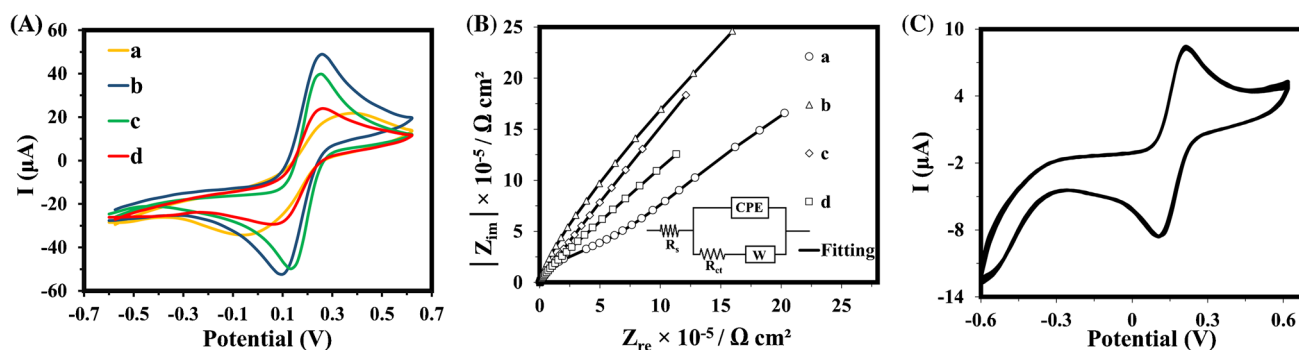
Fig. 2 A CVs and **B** EISs of the different electrodes (a) GCE, (b) PBA-Au-MXene QD/GCE, (c) ssDNA/PBA-Au-MXene QD/GCE, (d) dsDNA/PBA-Au-MXene QD/ and **C** CVs of PBA-Au-MXene QD/GCE following a series of scans for 40 cycles GCE (5mM $[Fe(CN)_6]^{3-/4-}$ containing 0.1 M KCl)

the Randles-Sevich formula, the effective surface areas of GCE and PBA-Au-MXene QD/GCE were calculated to be 0.013 ± 0.00021 cm^2 and 0.040 ± 0.00078 cm^2, respectively. The results are consistent with those shown in Fig. S1G and demonstrate that PBA-Au-MXene QD has significantly increased the electrode's effective surface area for immobilizing probes for eventual diagnosis. Parameter n is an identification valid for the uniformity of the double layer acquired utilizing the EIS approach, and it can range from 0 to 1 [30], indicating material morphology. n for GCE, PBA-Au-MXene QD/GCE, ssDNA/PBA-Au-MXene QD/GCE, and dsDNA/PBA-Au-MXene QD/GCE are equal to 0.8, 0.99, 0.95, and 0.94, respectively which is compatible with the AFM study.

In addition, to assess the stability of the binding between PBA-Au-MXene QD and GCE, the modified GCE was subjected to 40 consecutive scans with CVs at a rate of 50 mV.s^{-1}. The results indicate that there were no significant changes in either oxidation/reduction potential or current for the PBA-Au-MXene QD-modified GCE (Fig. 2C). This suggests that the interface between PBA-Au-MXene QD and GCE is highly stable, which is advantageous for the development of electrochemical biosensor.

Optimizing experimentation conditions

To develop a biosensor with excellent sensitivity and selectivity several affecting elements, including MXene QD concentration, electrodeposition time, prob concentration and time stability, temperature, pH, time hybridization, and so on were explored.

Based on the results presented in Fig. S3A, there was no significant difference between the miRNA-122 synthetic sample and serum samples treated with proteinase K (without complete extraction of miRNA). Therefore, the optimized steps were carried out using the treated serum. This was because the proposed sensor was able to effectively detect the treated serum in real conditions. The impacts

of essential agents, such as MXene QD concentrations (Fig. S3B) and electrodeposition durations (Fig. S3C) were tested and optimized for biosensor platform development. According to the presented results in the supplemental file, the optimal conditions are 8000 mg/mL of MXene QD and 300 s of electrodeposition time.

The thickness of the PBA-Au-MXene QD layer, which is the same as the diffusion length (L), can be obtained from the following Eq. (1) [31]:

$$\omega = \frac{D}{L^2} \tag{1}$$

In the above equation, ω is characteristic of diffusion in a finite layer, and D is the diffusion coefficient. Accordingly, the L value was calculated to be 0.00032 ± 0.000001 cm.

The probe concentrations were optimized after the GCE was modified using PBA-Au-MXene QD nanocomposites. The effect of probe concentration on detection was investigated, with concentrations ranging from 1 to 1000 nM in 5 mM $[Fe(CN)_6]^{3-/4-}$ solution comprising 0.1 M KCl (Fig. S3D). A weak response signal at concentrations less than 500 nM may be due to an insufficient amount of immobilized probe on the GCE, whereas a reduction in response signal at concentrations greater than 500 nM may be due to the impact of the additional mass of immobilized probe. As a result, 500 nM was chosen as the best probe concentration [32].

The probe's immobilized period on the modified GCE was measured between 1 and 15 h. The DPV answer increased with an immobilization time of up to 9 h. After, there was no substantial increase in the signal's responsiveness ((Fig. S3E). As a result, a 9 h immobilization duration was chosen to ensure optimal probe immobilization in the modified GCE.

Fig. S3F and G show the pH influence on probe immobilization and the hybridization process on biosensor performance, respectively. At a pH less than 7.4, the ssDNA

phosphodiesterase chain protonated, lowering the solubilization of ssDNA molecules and thus the DNA hybridization process. At a pH of more than 7.4, the buffer denatured the dsDNA helical structure by breaking the weak hydrogen bonds between the nucleobases. As a result, the ideal pH for biosensing was confirmed to be 7.4.

The relevance of hybridized time in biosensing instances for detection accuracy is understood. The optimum miR-122 hybridized time on ssDNA/PBA-Au-MXene QD/GCE varied from 30 to 180 min. According to Fig. S3H, the DPV peak current peaked at 60 min. The DPV answer was not significantly changed by developing hybridized time.

The hybrid temperature was investigated between 10 and 55 °C. The response signal dropped with a continual rise in hybrid temperature after just a hybrid temperature of 25 °C (Fig. S3I). Increasing temperatures reduce hybrid efficiency. As a result, in the next experiments, 25 °C was used to hybridize the probe with miR-122. Therefore, the results obtained from the optimization process were used to continue with the subsequent steps.

The biosensor's selectivity, stability, repeatability, approach, and sensitivity

To analyze the selectivity of the biosensor, DPV responses were evaluated after the hybridization of the ssDNA probe with different types of sequences at a concentration of 1 pM. These sequences included the complementary sequence, as well as sequences with 2, 5, and 9 base mismatches and non-complementary. The results of Fig. 3A revealed that the biosensor had the highest response to the complementary sequence and its response decreased as the number of mismatched bases increased. Interestingly, the response to the non-complementary sequence was similar to that of a blank sample without any miR-122. Furthermore, there was no significant difference in response among the synthetic miR-122 sample and serum, which were obtained without complete extraction of miRNA.

The stability of the biosensor was also evaluated over a longer time. To do so, a group of fabricated biosensors was stored at 4 °C for up to 42 days. After each step of hybridization and detection, dsDNA hybrid structures of
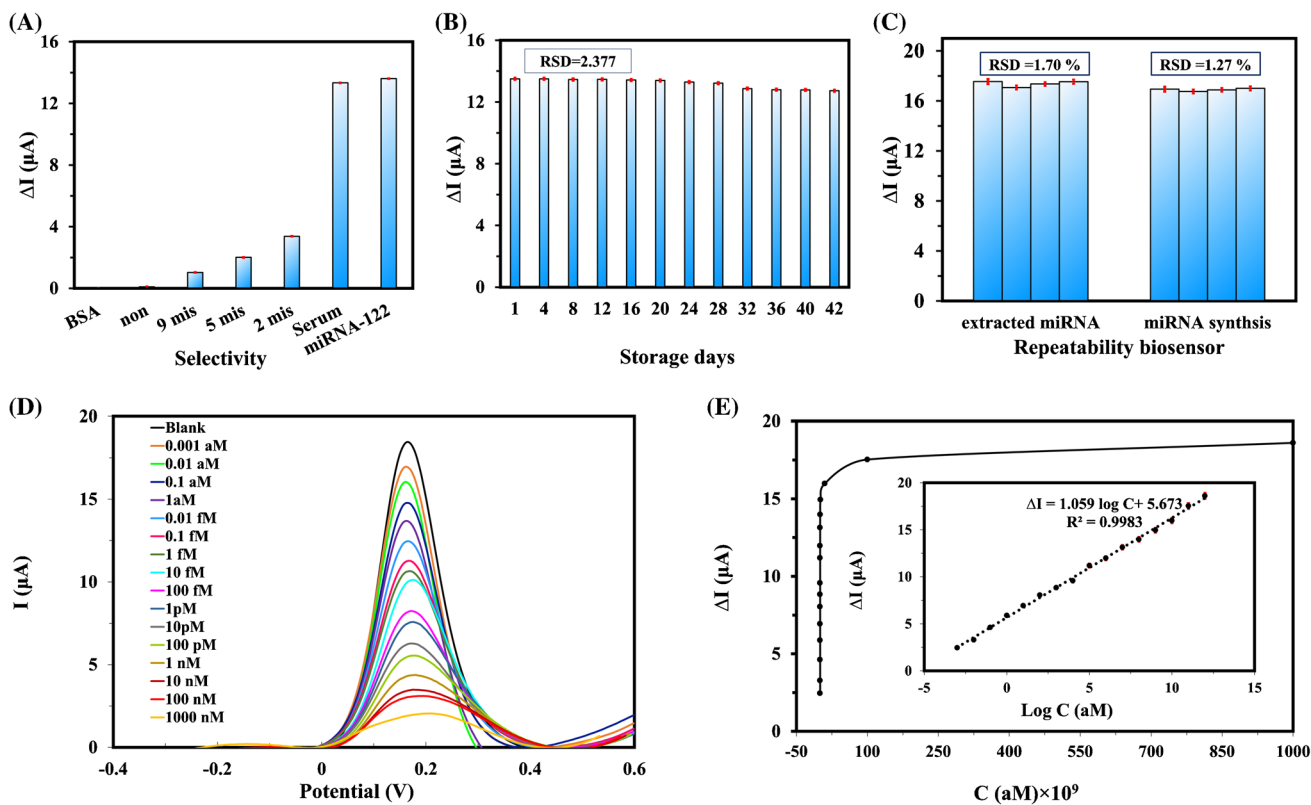
Fig. 3 A The sensitivity of the biosensor for non-complementary, 9, 5, 2-mismatch, and miR-122 sequences, **B** the biosensor's stability after being stored for 42 days; **C** Biosensor reproducibility evaluation with four-time measurement at 1 pM concentration in miRNA synthesized and extracted samples ($n=3$), **D** DPV signals at a 5mM [Fe(CN)$_6$]$^{3-/4-}$ containing 0.1 M KCl for different miR-122 concentrations, and **E** the corresponding calibration curves for log C (aM) vs. DPV responses in the wide range of 0.001 aM to 1000 nM (the error bars indicate the standard deviation estimated by three independent measurements). (Inset: the DPV reply of the biosensor among -0.2 to 0.4, where the scan rate was 50 mV.s^{-1} in a 5 mM [Fe(CN)$_6$]$^{3-/4-}$ a solution containing 0.1 M KCl, $n=3$)

dsDNA/PBA-Au-MXene QD/GCE were denaturized in a 0.5 M NaOH solution, followed by room-temperature drying. Finally, new serum samples were detected with biosensors. According to Fig. 3B, the biosensors remained stable throughout the 42 days. After 42 days, the biosensors maintained 94.26% of their initial response. These findings suggest that the offered biosensor has promising stability. Based on these results, it can be concluded that the reversibility of the biosensor is 11 times. These findings suggest that the offered biosensor has promising stability and reversibility.

A repeatability study was performed to determine the closeness between the results measured by the biosensor at a concentration of 1 pM miRNA-122 (synthesized and extracted) with three replicates ($n = 3$). Based on the bar graph, there was no significant difference in the ΔI value of the two separate sets under test (Fig. 3C). The biosensor's repeatability, with a standard deviation (%RSD) in the range of 1.27–1.70%, indicates its high repeatability.

Finally, the designed biosensor was analyzed by hybridizing with different concentrations of synthesized miR-122 in standard solution as shown in Fig. 3D. The current changes (ΔI), which is the difference among the peak height of the ssDNA/PBA-Au-MXene QD/GCE and the reaction of hybridizing, increased with the target concentration. This change showed acceptable linear dependence with the target concentration logarithm in the wide range from 0.001 aM to 1000 nM (Fig. 3E). The linear equation and LOD for this response was $\Delta I = 1.059 \log C + 5.673$ and 0.00081 ± 0.000105 aM (0.8 zM). LOD was calculated based on the 3SD/m equation.

To assess the biosensor's sensitivity, 500 nM of the ssDNA probe was immobilized on the PBA-Au-MXene QD/GCE, and the biosensor assessed miR-122 at different concentrations ranging from 0.001 aM to 1000 nM. Using the following formula, the biosensor's sensitivity was determined.
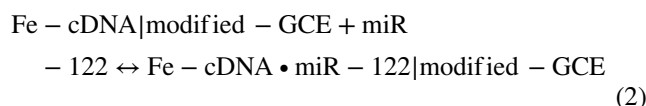
$$sensivity = \frac{slpoe\ of\ calibration\ plot\left(\mu A a M^{-1}\right)}{active\ surface\ area\left(cm^2\right)}$$

Based on the calibration plots shown in Fig. 3E, the biosensor's sensitivity was determined to be 26.47 $\mu AaM^{-1}cm^{-2}$. The very sensitive miR-122 assay is linked to the miR-122 biosensor based on R2 values and sensitivity.

Table.S2 provides a comparison of the effectiveness of different methods for detecting miR-122. The results presented in this table demonstrate that the introduced biosensor in the study has a broader linear range and superior LOD compared to other biosensors developed for quantifying miR-122.

Determination of the binding affinity between miR-122 and Fe-cDNA immobilization

A fundamental presumption of cDNA probe-based biosensors is that a stable structure forms when the probe interacts with the target. Nevertheless, the strength of the interaction between the probe and the target is poorly understood, particularly when the reaction occurs on a GCE surface composed of multiple layers. In this part, a Langmuir model is utilized to calculate the binding constant between probe cDNA and miR-122. Figure 4A displays the correlation among ΔI and miR-122 concentrations across a broad concentration span. The initial rise in ΔI is steep, but it eventually levels off a comparatively constant amount at higher concentrations. If the cDNA-miR-122 hybridization conforms to the criteria of the Langmuir isotherm model, the binding affinity (also known as the equilibrium constant K_b) can be formulated as (Eqs. 2 and 3) [33]:

$$\begin{aligned} Fe - cDNA|modified - GCE + miR \\ - 122 \leftrightarrow Fe - cDNA \bullet miR - 122|modified - GCE \end{aligned} \tag{2}$$

$$K_b = \frac{[Fe - cDNA \bullet miR - 122|modified - GCE]}{[Fe - cDNA|modified - GCE][miR - 122]} \tag{3}$$

The terms [Fe-cDNA• miR-122 $|$ modified-GCE], [Fe-cDNA $|$ modified-GCE], and [miR-122] refer to the level of concentration of the cDNA-miR-122 hybridization on the modified-GCE, the concentration of the probe Fe-cDNA (Fe symbols is [Fe(CN$_6$)]$^{3-/4-}$ solution comprising 0.1 M KCl and cDNA symbol is ssDNA probe) immobilization on the modified-GCE, and the miR-122 concentration, respectively. As a result, the correlation among ΔI, the ΔI_{max} (maximum ΔI) that corresponds to the highest miR-122 concentration at saturant hybridization, the miR-122 concentration [miR-122], and K_b (binding constant) can be represented as follows (Eq. 4):

$$\Delta I = \Delta I_{max} \times \frac{k_b[miR - 122]^n}{1 + k_b[miR - 122]^n} \tag{4}$$

It is possible to reorganize this formula to obtain Eq. 5:

$$\frac{[miR - 122]^n}{\Delta I} = \frac{1}{k_b . \Delta I_{max}} + \frac{[miR - 122]^n}{\Delta I_{max}} \tag{5}$$

The value of parameter n relates to the distribution of level energy [34]. When using the Langmuir isotherm model, n nears 1, indicating a homogeneous surface.

Through nonlinear fitting of the experimental data, it is demonstrated that the Langmuir model (Eq. 4, $n = 1$) could be used in this instance (Fig. 4A) to provide the following values (Fig. 4B): $\Delta I_{max} = 18.62$, $K_b = 1.79 \times 10^{-9}$

Fig. 4 Langmuir isotherms are generated by interactions between the miR-122 biosensor and different concentrations of miR-122. **A** The Langmuir isotherm model's nonlinear fit of the experimental data and **B** the Langmuir isotherm model provide a linear fit to the experimental data
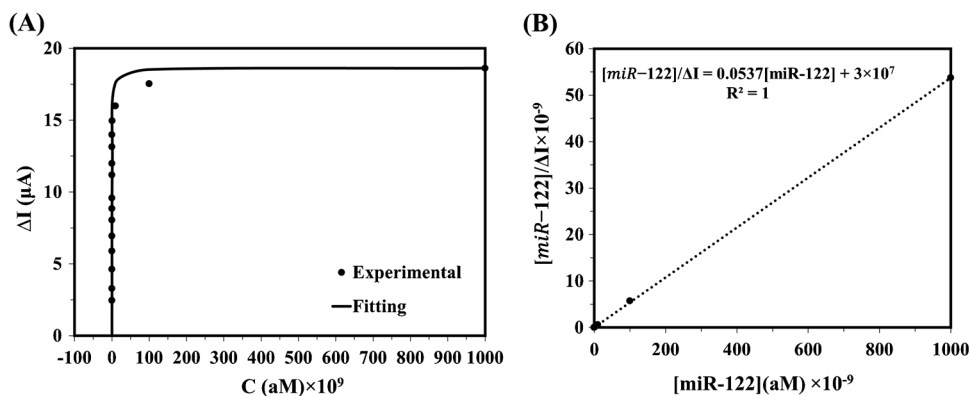
aM^{-1}, and $n = 1$. Equation (5) indicates that the ratio of [miR-122]^n. The intercept of this relationship is plotted with $n = 1$, which was determined through nonlinear fitting in a previous analysis. The results from this plot match well with those gained from Fig. 4B, confirming the validity of the calculated ΔI_{max} and K_b amounts. The significant K_b amount of 1.79×10^{-9} aM^{-1} or 1.79×10^9 M^{-1} indicates that the surface-bound probe cDNA can attach firmly to the 22 mer miR-122 in the given experimental situation. This firm binding is likely due to the biosensor's lower LOD and a broad range of detectable quantities.

Biosensing approach in clinical testing

The effectiveness of using biosensors for clinical trials was evaluated by conducting tests on 30 miRNA samples, with and without extraction, from serum samples. The samples were taken from 15 negative and 15 positive BC samples. All 15 positive samples showed a significant response ($\Delta I > 7.96$ and 7.93 µA for serum and extracted miRNA, respectively). While, the response of all 15 negative samples was relatively low ($\Delta I < 4.75$ and 4.65 µA for serum and extracted miRNA, respectively), showing that the serum's miRNA concentrations were normal (Fig. 5A).

According to Fig. 5B, D, and E, the findings of 30 sample analyses were recorded in a box diagram for further investigation. A *t*-test was also performed to ascertain the significance of the difference between the negative and positive categories. When comparing the data, differences of significance were seen for three approaches between the two groups (p about 0.0001). Additionally, ROC curves ("receptor operating characteristics") were utilized to evaluate the capability of distinguishing the suggested approach and compare it with RT-qPCR (as shown in Fig. 5C, D, and E). The IUPAC way [35] was utilized to establish the cutoff values for the identified threshold values of the suggested biosensor for both miRNAs with and without extraction, as well as for RT-qPCR. These cutoff values were $\Delta I > 5.711$, $\Delta I > 6.517$, and $\Delta C_t < -4.856$, respectively. As a result, for the biosensor

technique, an ΔI value greater than 5.711 and 6.517 was designated as indicating BC patients for miRNA detection with and without extraction, respectively, whereas an ΔI value less than these thresholds was indicative of healthy Persons. On the other hand, for the RT-qPCR technique, a ΔC_t value greater than -4.856 was indicative of healthy individuals, whereas a value less than this threshold was persons of BC patients. Based on the ROC curve-derived cutoffs, the biosensor method did not produce any false results, while the RT-qPCR technique had three false positives and three false negatives. Hence, the findings validate the accuracy of the diagnosis ability of the biosensor even in real serum samples.

The AUC (area under the curve) was calculated using three different approaches, and it demonstrates the outstanding specificity and precision of the provided biosensor to discriminate between samples with and without BC. The created biosensor has 100% sensitivity, 100% specificity, and an AUC of 1, and it can detect real clinical samples both with and without miR-122 extraction. The diagnostic usefulness of miR-122 in distinguishing between the control and case groups was also demonstrated by RT-qPCR diagnosis, which had 80% sensitivity, 80% specificity, and an AUC of 0.81 (Fig. S4A, B, and C). As a consequence, the finding demonstrates that the biosensor approach has greater specificity and sensitivity than the RT-qPCR method.

The novel aspect of this research was the development of a biosensor utilizing Au-MXene QD nanoparticles that enabled the conversion of a non-conductive polymer into a conductive composite via the electrodeposition method. The study's findings revealed that the presence of any interfering species in the matrices without extracted miRNA did not significantly affect the accuracy of miR-122 detection using the proposed biosensor. This suggests that the biosensor can reliably diagnose miR-122 in various real samples without requiring extraction and separate processing. Moreover, the biosensor could accurately differentiate between patient and healthy specimens.

The proposed biosensor offers several inherent benefits over other biosensors developed for detecting BC. Firstly,
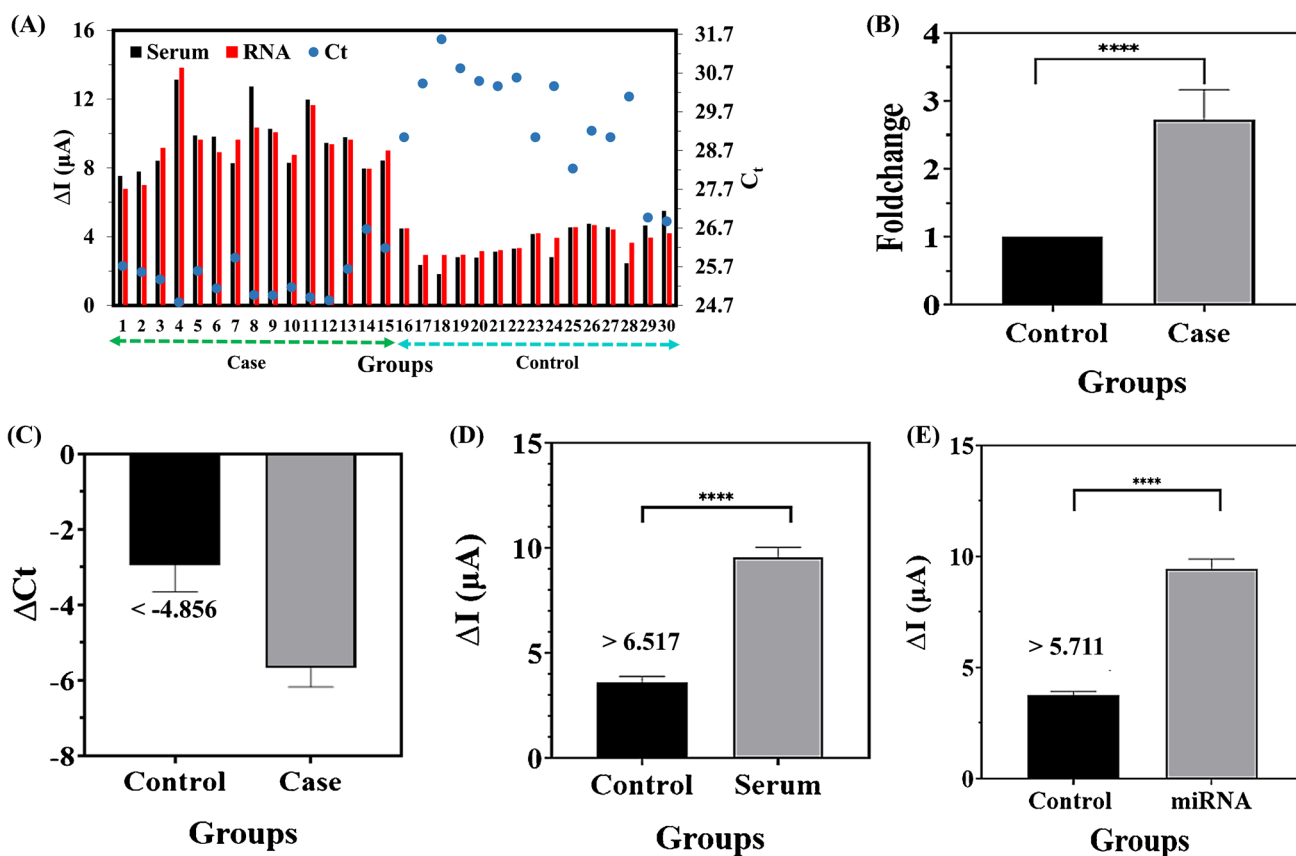
Fig. 5 A Rod curves of BC miRNA diagnosis in 30 real samples using RT-qPCR and DPVs response with and without miRNA extraction, **B**, **C**, **D**, and **E** the analogy of ΔI and expression severity of case (15 samples) and control samples (15 samples) of BC with RT-qPCR and biosensor technique

the biosensor is capable of detecting miR-122 with low expression levels quantitatively, with a limit of detection at the zM level for both synthetic and real samples. Secondly, the designed biosensor demonstrated a meaningful difference between the control and case categories with 100% sensitivity and 100% specificity. Finally, the developed biosensor was able to quantify miR-122 even in the presence of invasive species in the matrices without the need for extraction of miRNA.

Conclusion

This miR-122 biosensor was manufactured using PBA-Au-MXene QD nanocomposite. This method could be applied to PBA as a non-conductive polymer transformed into a conductive composite by incorporating Au-MXene QD. Then the thiolated ssDNA probe was covalently fixed to the nanocomposite surface with thiol-Au bonds. This study describes the development of an ultrasensitive biosensor for detecting miR-122, a biomarker for breast cancer. The biosensor detected miR-122 with high sensitivity, low LOD, and a wide linear diagnosis range. Comparing miR-122 detection with and without miR-122 extraction and RT-qPCR in 30 clinical samples demonstrated the biosensor's accuracy and reproducibility. This innovative biosensor showed high potential for breast cancer diagnosis and improved health outcomes. This was due to its ability to diagnose very low miR-122 levels without complicated pretreatment steps. In addition, the technology presented has potential for application to microfluidics, wearable biosensors, and portable electronics, which enhance point-of-care sensing. This research presents a significant step toward developing rapid, accurate, and noninvasive clinical tools for breast cancer diagnosis.

Declarations

Competing interests The authors declare no competing interests.

References

1. Mohammadi M, Goodarzi M, Jaafari M, Mirzaei H, Mirzaei H (2016) Circulating microRNA: a new candidate for diagnostic biomarker in neuroblastoma. Cancer Gene Ther 23(11):371–372

2. Wozniak MB, Scelo G, Muller DC, Mukeria A, Zaridze D, Brennan P (2015) Circulating microRNAs as non-invasive biomarkers for early detection of non-small-cell lung cancer. PLoS ONE 10(5):e0125026

3. Saleh AA, Soliman SE, Habib MSE-d, Gohar SF, Abo-Zeid GS (2019) Potential value of circulatory microRNA122 gene expression as a prognostic and metastatic prediction marker for breast cancer. Mol Biol Rep 46:2809–2818

4. Fong MY, Zhou W, Liu L, Alontaga AY, Chandra M, Ashby J et al (2015) Breast-cancer-secreted miR-122 reprograms glucose metabolism in premetastatic niche to promote metastasis. Nat Cell Biol 17(2):183–194

5. El-Khoury V, Pierson S, Kaoma T, Bernardin F, Berchem G (2016) Assessing cellular and circulating miRNA recovery: the impact of the RNA isolation method and the quantity of input material. Sci Rep 6(1):19529

6. El Aamri M, Yammouri G, Mohammadi H, Amine A, Korri-Youssoufi H (2020) Electrochemical biosensors for detection of microRNA as a cancer biomarker: Pros and cons. Biosensors 10(11):186

7. Hatamluyi B, Lorestani F, Es'haghi Z (2018) Au/Pd@ rGO nanocomposite decorated with poly (L-cysteine) as a probe for simultaneous sensitive electrochemical determination of anticancer drugs, Ifosfamide and Etoposide. Biosens Bioelectron 120:22–29

8. Mittal S, Kaur H, Gautam N, Mantha AK (2017) Biosensors for breast cancer diagnosis: a review of bioreceptors, biotransducers and signal amplification strategies. Biosens Bioelectron 88:217–231

9. Ranjbari S, Darroudi M, Hatamluyi B, Arefinia R, Aghaee-Bakhtiari SH, Rezayi M et al (2022) Application of MXene in the diagnosis and treatment of breast cancer: a critical overview. Front Bioeng Biotechnol 10:984336

10. Ebrahimi A, Nikokar I, Zokaei M, Bozorgzadeh E (2018) Design, development and evaluation of microRNA-199a-5p detecting electrochemical nanobiosensor with diagnostic application in Triple Negative Breast Cancer. Talanta 189:592–598

11. Liu L, Zhu S, Wei Y, Liu X, Jiao S, Yang J (2019) Ultrasensitive detection of miRNA-155 based on controlled fabrication of AuNPs@ MoS2 nanostructures by atomic layer deposition. Biosens Bioelectron 144:111660

12. Ranjbari S, Rezayi M, Arefinia R, Aghaee-Bakhtiari SH, Hatamluyi B, Pasdar A (2023) A novel electrochemical biosensor based on signal amplification of Au HFGNs/PnBA-MXene nanocomposite for the detection of miRNA-122 as a biomarker of breast cancer. Talanta 255:124247

13. Miao P, Wang B, Yu Z, Zhao J, Tang Y (2015) Ultrasensitive electrochemical detection of microRNA with star trigon structure and endonuclease mediated signal amplification. Biosens Bioelectron 63:365–370

14. Meinderink D, Orive A, Grundmeier G (2018) Electrodeposition of poly (acrylic acid) on stainless steel with enhanced adhesion properties. Surf Interface Anal 50(11):1224–1229

15. Smith DA, Newbury LJ, Drago G, Bowen T, Redman JE (2017) Electrochemical detection of urinary microRNAs via sulfonamide-bound antisense hybridisation. Sens Actuators, B Chem 253:335–341

16. Khodadoust A, Nasirizadeh N, Seyfati SM, Taheri RA, Ghanei M, Bagheri H (2023) High-performance strategy for the construction of electrochemical biosensor for simultaneous detection of miRNA-141 and miRNA-21 as lung cancer biomarkers. Talanta 252:123863

17. Mahmood M, Rasheed A, Ayman I, Rasheed T, Munir S, Ajmal S et al (2021) Synthesis of ultrathin MnO2 nanowire-intercalated 2D-MXenes for high-performance hybrid supercapacitors. Energy Fuels 35(4):3469–3478

18. Lee E, VahidMohammadi A, Prorok BC, Yoon YS, Beidaghi M, Kim D-J (2017) Room temperature gas sensing of two-dimensional titanium carbide (MXene). ACS Appl Mater Interfaces 9(42):37184–37190

19. Enríquez JMH, Lajas LAC, Alamilla RG, Alamilla PG, Handy EB, Galindo GC, Serrano LAG (2013) Synthesis of solid acid catalysts based on TiO2-SO42-and Pt/TiO2-SO42-applied in n-hexane isomerization. Open J Metal 2013(3):34–44

20. Khan AR, Husnain SM, Shahzad F, Mujtaba-ul-Hassan S, Mehmood M, Ahmad J et al (2019) Two-dimensional transition metal carbide (Ti 3 C 2 T x) as an efficient adsorbent to remove cesium (Cs+). Dalton Trans 48(31):11803–11812

21. Li Y, Sun XS (2015) Synthesis and characterization of acrylic polyols and polymers from soybean oils for pressure-sensitive adhesives. RSC Adv 5(55):44009–44017

22. Yılmaz O, Özkan ÇK, Yılmaz CN, Yorgancıoğlu A, Özgünay H, Karavana HA (2017) Synthesis and characterization of functional acrylic copolymers via RAFT mini-emulsion polymerization. AIP Confer Proc 1918(1):020006

23. Wang G (2011) Synthesis of poly (n-butyl acrylate) homopolymers by activators generated by electron transfer (AGET) ATRP using FeCl3· 6H2O/succinic acid catalyst. Iran Polym J 20(11):931–938

24. Oh SJ, Lee SC, Park SY (2006) Photopolymerization and photobleaching of n-butyl acrylate/fumed silica composites monitored by real time FTIR-ATR spectroscopy. Vib Spectrosc 42(2):273–277

25. Tsekenis G, Chatzipetrou M, Tanner J, Chatzandroulis S, Thanos D, Tsoukalas D et al (2012) Surface functionalization studies and direct laser printing of oligonucleotides toward the fabrication of a micromembrane DNA capacitive biosensor. Sens Actuators, B Chem 175:123–131

26. Manzano M, Viezzi S, Mazerat S, Marks RS, Vidic J (2018) Rapid and label-free electrochemical DNA biosensor for detecting hepatitis A virus. Biosens Bioelectron 100:89–95

27. Chen Y, Wang A-J, Yuan P-X, Luo X, Xue Y, Feng J-J (2019) Three dimensional sea-urchin-like PdAuCu nanocrystals/ferrocene-grafted-polylysine as an efficient probe to amplify the electrochemical signals for ultrasensitive immunoassay of carcinoembryonic antigen. Biosens Bioelectron 132:294–301

28. Zare H, Meshkat Z, Hatamluyi B, Rezayi M, Ghazvini K, Derakhshan M et al (2022) The first diagnostic test for specific detection of Mycobacterium simiae using an electrochemical label-free DNA nanobiosensor. Talanta 238:123049

29. Hatamluyi B, Sadeghian R, Sany SBT, Alipourfard I, Rezayi M (2021) Dual-signaling electrochemical ratiometric strategy for simultaneous quantification of anticancer drugs. Talanta 234:122662

30. Hryniewicz BM, Volpe J, Bach-Toledo L, Kurpel KC, Deller AE, Soares AL et al (2022) Development of polypyrrole (nano) structures decorated with gold nanoparticles toward immunosensing for COVID-19 serological diagnosis. Mater Today Chem 24:100817

31. Nguyen TQ, Breitkopf C (2018) Determination of diffusion coefficients using impedance spectroscopy data. J Electrochem Soc 165(14):E826–E831

32. Eskandari M, Faridbod F (2018) A printable voltammetric genosensor for tumour suppressor gene screening based on a nanocomposite of Ceria NPs–GO/nano-PANI. New J Chem 42(19):15655–15662

33. Lu L, Liu C, Miao W, Wang X, Guo G (2020) Ultrasensitive detection of miRNA based on efficient immobilization of probe and electrochemiluminescent quenching of Ru (bpy) 32+ by methylene blue. Anal Chim Acta 1093:52–60

34. Kapoor A, Ritter J, Yang RT (1990) An extended Langmuir model for adsorption of gas mixtures on heterogeneous surfaces. Langmuir 6(3):660–664

35. Hatamluyi B, Rezayi M, Jamehdar SA, Rizi KS, Mojarrad M, Meshkat Z et al (2022) Sensitive and specific clinically diagnosis of SARS-CoV-2 employing a novel biosensor based on boron nitride quantum dots/flower-like gold nanostructures signal amplification. Biosens Bioelectron 207:114209